Molecular Cancer Therapeutics

AZD5153: A Novel Bivalent BET Bromodomain Inhibitor Highly Active against Hematologic Malignancies

Garrett W. Rhyasen[1], Maureen M. Hattersley[1], Yi Yao[1], Austin Dulak[1], Wenxian Wang[1], Philip Petteruti[1], Ian L. Dale[2], Scott Boiko[1], Tony Cheung[1], Jingwen Zhang[1], Shenghua Wen[1], Lillian Castriotta[1], Deborah Lawson[1], Michael Collins[1], Larry Bao[1], Miika J. Ahdesmaki[2], Graeme Walker[2], Greg O'Connor[1], Tammie C. Yeh[1], Alfred A. Rabow[2], Jonathan R. Dry[1], Corinne Reimer[1], Paul Lyne[1], Gordon B. Mills[3], Stephen E. Fawell[1], Michael J. Waring[2], Michael Zinda[1], Edwin Clark[1], and Huawei Chen[1]

Abstract

The bromodomain and extraterminal (BET) protein BRD4 regulates gene expression via recruitment of transcriptional regulatory complexes to acetylated chromatin. Pharmacological targeting of BRD4 bromodomains by small molecule inhibitors has proven to be an effective means to disrupt aberrant transcriptional programs critical for tumor growth and/or survival. Herein, we report AZD5153, a potent, selective, and orally available BET/BRD4 bromodomain inhibitor possessing a bivalent binding mode. Unlike previously described monovalent inhibitors, AZD5153 ligates two bromodomains in BRD4 simultaneously. The enhanced avidity afforded through bivalent binding translates into increased cellular and antitumor activity in preclinical hematologic tumor models. *In vivo* administration of AZD5153 led to tumor stasis or regression in multiple xenograft models of acute myeloid leukemia, multiple myeloma, and diffuse large B-cell lymphoma. The relationship between AZD5153 exposure and efficacy suggests that prolonged BRD4 target coverage is a primary efficacy driver. AZD5153 treatment markedly affects transcriptional programs of MYC, E2F, and mTOR. Of note, mTOR pathway modulation is associated with cell line sensitivity to AZD5153. Transcriptional modulation of MYC and HEXIM1 was confirmed in AZD5153-treated human whole blood, thus supporting their use as clinical pharmacodynamic biomarkers. This study establishes AZD5153 as a highly potent, orally available BET/BRD4 inhibitor and provides a rationale for clinical development in hematologic malignancies. *Mol Cancer Ther; 15(11); 2563–74. ©2016 AACR.*

Introduction

BRD4 is a member of the bromodomain and extraterminal (BET) family of chromatin reader proteins. BET proteins feature characteristic tandem N-terminal bromodomains that function to interact with N-acetyl lysine residues on histones and nuclear proteins (1–4). Bromodomain-mediated interactions localize BRD4 to discrete chromosomal locations, facilitating the recruitment of transcriptional regulatory complexes, such as the general initiation cofactor Mediator and the Positive Transcription Elongation Factor b (P-TEFb; refs. 5–7). Studies involving chromatin immunoprecipitation coupled with DNA-sequencing (ChIP-seq) have revealed a highly asymmetric genome-wide binding pattern of BRD4, with most chromatin-bound BRD4 localizing to enhancer elements. In particular, BRD4 has been shown to predominately bind enhancer elements, which are important for cell-type specification and oncogenesis (8, 9).

The discovery of lysine-mimetic small molecules capable of disrupting the chromatin binding activity of BET bromodomains was a crucial step toward uncovering the cancer-supporting activity of BRD4 (10–12). In hematologic malignancies, such as acute myeloid leukemia (AML), multiple myeloma (MM), and diffuse large B-cell lymphoma (DLBCL), the misregulated expression of hematopoietic transcription factors is particularly important. BRD4 maintains and facilitates oncogenic transcription by interacting directly with transcription factors, and/or co-occupying transcription factor gene control loci, contributing to cancer cell proliferation and survival. For example, in AML, BRD4 chromatin occupancy is enriched at enhancer and promoter regions and highly correlated with the distribution of PU.1, FLI1, ERG, C/EBPα, C/EBPβ, and MYB (13). BRD4 inhibition interferes with the functional output of these lineage-specific transcription factors, and thereby inhibits AML maintenance. In MM, the survival of malignant plasma cells is dependent on MYC transcriptional activity. MYC deregulation in MM can occur through gene translocation, amplification, and overexpression (14, 15). In this

[1]Oncology Innovative Medicines Unit, AstraZeneca R&D Boston, Waltham, Massachusetts. [2]AstraZeneca, Macclesfield, Cheshire, UK. [3]Department of Systems Biology, The University of Texas MD Anderson Cancer Center, Houston, Texas.

Note: Supplementary data for this article are available at Molecular Cancer Therapeutics Online (http://mct.aacrjournals.org/).

G.W. Rhyasen and M.M. Hattersley share first authorship of this article.

Corresponding Author: Huawei Chen, Oncology Innovative Medicines Unit, AstraZeneca R&D Boston, 35 Gatehouse Drive, Waltham, MA 02451. Phone: 781-839-4417; Fax: 781-839-4200; E-mail: raymond.chen@astrazeneca.com

doi: 10.1158/1535-7163.MCT-16-0141

setting, BRD4 inhibition disrupts MYC activity and results in MM cell-cycle arrest and senescence (16). DLBCL is a biologically and clinically heterogeneous disease, which is similarly typified by the activation of lineage-specific and growth-associated transcription factors, including NF-κB, BCL6, p53, and MYC (17–20). BRD4 inhibition downregulates oncogenic MYC and E2F transcriptional pathways, resulting in antiproliferative effects across DLBCL subtypes (21). Based on this and other work, several drug candidates targeting BRD4/BET have progressed into clinical trials to treat Nut Midline Carcinoma (NMC), AML, myelodysplastic syndromes (MDS), MM, DLBCL, glioblastoma multiforme, and other solid tumors.

We recently described the discovery of BET bromodomain inhibitors that are chemically distinct from the commonly described benzodiazepine-based scaffold and capable of a novel bivalent binding mode (22). A dedicated medicinal chemistry campaign led to the discovery of a BET inhibitor clinical candidate AZD5153 (23). In this study, we characterize the in cell bivalent binding mode of AZD5153 and demonstrate the cellular and pharmacological advantages achieved through the unique biophysical properties of AZD5153 using AML, MM, and DLBCL as model systems.

Materials and Methods

Cell lines and reagents

Most of cell lines were purchased from ATCC or DSMZ and a few obtained from academic laboratories from 2006 to 2014, and cultured according to providers' instructions (detailed information in Supplementary Table S1). Cell lines were authenticated using DNA fingerprinting short-tandem repeat (STR) assays and confirmed to be free of bacterial and viral contaminations by IDEXX. All cell lines were used within 15 passages, and less than 6 months. Antibodies used for Western blot analysis were from Cell Signaling Technology: Anti-cMyc (#5605), anti-GAPDH (#2118), anti-phospho-p70S6K (T389/412; #9209), anti-p70S6K (#2708), anti-PRAS40 (#2610), anti-phospho-S6 (S235/236; #4856), anti-S6 (#2217), anti-phospho-4EBP1 (S65; #9451), and anti-4EBP1 (#9644).

Bioluminescence resonance energy transfer (BRET) NanoBRET assay

The BRD4 NanoBRET assays have been previously described (24). Briefly, the expression construct of Histone H3.3-Halotag (NM_002107) was cotransfected with either NanoLuc-BRD4 full-length (1-1362; 060885), NanoLuc-BRD4 full-length N433F mutant, or NanoLuc-N-terminal BRD4-BD1 (amino acids 44–168) expression vector into HCT116 cells. Cells were then seeded into 384-well plates and treated with various concentrations of compounds. Plates were read after 18 hours of compound treatment.

Immunofluorescent assays for BRD4 chromatin displacement

The Immuno-fluorescent assays have been previously described (22). Briefly, BRD4 foci were stained by using anti-BRD4 antibody (Sigma Aldrich, HPA015055) and secondary anti-rabbit antibody labeled with Alexa Fluor 488. The specificity of BRD4 antibody was verified by siRNA BRD4 knockdown in U2OS cells (22). Image acquisition was carried out by ImageXpress MicroXL High Content Screening System (Molecular Devices) and data analysis by MetaXpress (Molecular Devices).

MYC flow assay

MM.1S cells were plated in 96-well plates at 200k cells/well and treated with serial concentrations of compound 1 hour after plating and grown for 16 hours at 37°C. Cells were transferred into a 96-well V-bottom plate and fixed sequentially with 2% paraformaldehyde for 10 minutes at 37°C followed with 90% cold methanol for 10 minutes on ice. Cells were washed and blocked in incubation buffer (PBS + 0.5%BSA) for 10 minutes and incubated with anti-cMyc primary antibody (1:200) at room temperature for 1 hour. Cells were washed twice and then stained with Alexa 488–conjugated anti-rabbit IgG (1:1000, Cell Signaling technology #4412) for 30 minutes at room temperature and washed again. The pellet was resuspended in incubation buffer and analyzed by flow cytometer (BD FACSCalibur) using the FL-1 detector. Data were analyzed using FlowJo software V7. Live-cell population was selected by gating on FCS/SSC and Geo Mean fluorescence of FL-1 signal was used to calculate IC_{50}.

Immunoblots

Cells were plated at 1×10^6 cells/mL in 6-well plates, and treated with compounds at various concentrations for 4 or 24 hours. Crude lysate was prepared with 1 × SDS lysis buffer (60 mmol/L Tris-HCl pH 6.8, 1% SDS, and 10% glycerol). For xenograft tumors, tissues were homogenized in buffer (20 mmol/L Tris pH 8.0, 150 mmol/L NaCl, 1 % NP-40, in 10 mL of lysis buffer supplement with 100 μL of Phosphatase Inhibitor Cocktail2 (Sigma Cat # P5726-5ML), 100 μL of Phosphatase Inhibitor Cocktail3 (Sigma Cat #P0044-5ML), 1 tablet of complete protease inhibitor cocktail (Roche #11836153001). Samples with 20 μg of total protein were loaded and Western blots were run following typical procedures.

Cell antiproliferation and viability assays

Sixty cell lines were cultured in appropriate medium. Optimal 384-well seeding densities were premeasured for linear growth over 72 hours. Thirty microliter cells/well was seeded in black, flat bottom 384-well plates and treated with compounds for 72 hours. The viable cells were measured using Alamar Blue reagents following manufacturer's protocol (Invitrogen). The percentage net growth is calculated by normalizing against the no-drug controls, and the GI_{50} value, the concentration that causes 50% net growth inhibition, was calculated using GraphPad Prism 6.

Viability assay was performed following the same protocol as the antiproliferation assay but differed in data treatment. Absolute number of remaining viable cells, instead of percentage net growth, was determined after 72 hours of compound treatment. Cell viability IC_{50} value was obtained by fitting the raw data points with sigmoidal nonlinear regression and IC_{50} curves were plotted using GraphPad Prism6.

FACS apoptosis assay

Apoptosis was analyzed by flow cytometry using CellEvent Caspase 3/7 Green detection reagent (ThermoFisher, #C10423). MV-4-11, MM.1S, and K562 cells were pretreated with AZD5153 or I-BET762 for 48 hours in culture media. Cells were collected and stained with 5 μmol/L final concentration of CellEvent for 30 minutes at 37°C. Flow cytometry was done on a BD Fortessa using the Blue laser and FITC filter set. Gating and data analysis were done using FlowJo V7.0 software.

RNA sequencing

After AZD5153 (200 nmol/L) or vehicle treatment of hematological cell lines (AML—KG1A, MOLM13, MV-4-11, OCIAML2; MM—IM9, MM.1S, MOLP8, OPM2, RPMI8226; DLBCL–OCILY19, WILL2) for 24 hours, RNA isolation, cDNA library generation, and sequencing to 12M reads on the Illumina HiSeq were carried out at Q^2 Solutions. Bcbio-nextgen was used to process FastQ files, perform quality control, alignment to genome build hg19, and quantify transcription expression based on Ensembl annotation. EdgeR [19910308] version 3.12.0 was used to identify differentially expressed genes using trimmed mean of M values for normalization and the exact test method for differential expression. All RNAseq data were deposited at GEO (GSE85840).

Gene set enrichment analysis

Gene set enrichment analysis (GSEA; 16199517 and 12808457) was performed using the GSEA software. A signal-to-noise preranked list of gene expression changes was generated from $\log_2$ FPKM values for vehicle and AZD5153-treated cell lines and compared with the hallmarks (h.all.v5.0.symbols.gmt) and transcription factor targets (c3.tft.v5.0.symbols.gmt) gene sets from MSigDb (16199517) using default parameters.

Reverse phase protein array (RPPA) for proteomic profiling

Proteomic profiling was carried out using high-density protein dot blot-based immunoassay system provided by Theranostics. Cells were treated with 200 nmol/L AZD5153 for 24 hours, protein lysates were prepared following Theranotics' protocol, and samples were shipped to Theranostics to perform the array study. A total of 182 endpoints were assessed by immunostaining with corresponding antibodies. Data acquisition, quality control, and normalization were performed by Theranostics. AZD5153-modulated protein targets were identified by performing a paired, two-sided Student *t* test between DMSO- and AZD5153-treated samples.

Quantitative PCR

Cell pellets containing $\sim 1 \times 10^6$ cells or $\sim$10 mg of tumor tissue were collected. RNA was extracted using an RNAeasy mini kit following manufacturer's protocol (Qiagen, cat# 74104). RNA was converted to cDNA with a High Capacity RT kit following manufacturer's protocol (Applied Biosystems, cat#4368814). PCR was performed using Taqman Gene Expression Master Mix (Applied Biosystems, cat#4369016) with 300 ng of cDNA and taqman probes (Applied Biosystems, #MYC-Hs00153408_m1, #HEXIM1-Hs00538918_s1, and #GAPDH control-4352934E) on ABI Prism 7900HT instrument.

Efficacy and PK/PD studies in xenograft models

Female CB17 SCID and SCID beige mice were obtained from Charles River and NSG mice from Jackson Labs. All animals were used in compliance with protocols approved by the Institutional Animal Care and Use Committees of AstraZeneca. Between 5×10^6 and 10^7 tumor cells were implanted into appropriate host mice and tumor volume was monitored twice weekly. Tumor volume (mm^3) is measured with calipers and calculated as $(W^2 \times L) / 2$, where W is width and L is length. Tumor growth inhibition (TGI) is calculated as $(RTV_{control} - RTV_{treatment})^*100) / (RTV_{control} - 1)$, where $RTV_{control}$ is the geometric mean of relative tumor volume of control group and $RTV_{treatment}$ is the treatment group. Relative tumor volume is calculated using final tumor volume/ initial tumor volume for individual animals. Statistical significance was evaluated using a one-tailed Student *t* test. Eight to ten mice per group were used for efficacy and three mice per group for PD studies. Mice were treated with either vehicle (0.5% hydroxymethylcellulose, 0.1% Tween80) or AZD5153 by oral gavage mini-pump infusion. For continuous administration of AZD5153, compound was solubilized in 20% v/v DMSO/60% v/v HP-B-CD in water, loaded into a mini pump (Alzet, model 2002) and implanted subcutaneously in mice. Tumor fragments collected were snap frozen or fixed in 10% buffered formalin. Blood samples were collected from the same mice and stabilized in EDTA. Plasma concentrations were determined by liquid chromatography/ tandem mass spectrometry method.

Immunohistochemical (IHC) analysis

Formalin-fixed tumors were subjected to processing through graded ethanol, xylene and paraffin, embedded into paraffin blocks, and 3-μm sections were cut for assays. IHC was run with an optimized protocol on the Ventana Discovery XT using anti-Myc primary rabbit polyclonal antibody (Millipore #06-340) at a 1:200 dilution, biotinylated anti-rabbit secondary antibody (Vector Labs #PK-6101) and the DABMap detection kit (Ventana Medical #760-124). For cleaved caspase-3, IHC was run with an optimized protocol on the Ventana Discovery XT using anti-Cleaved Caspase-3 primary rabbit polyclonal antibody (CST-9661) at a 1:5,000 dilution, biotinylated anti-rabbit secondary antibody (Vector Labs #PK-6101) and the DABMap detection kit (Ventana Medical #760-124). Digital slide images were acquired for both antibodies with the Aperio Scanscope XT using a 20X objective. Viable tumor areas were manually selected in Aperio Imagescope (version 11), and percent positive nuclei were quantified using a modified Nuclear Algorithm (version 9).

Modulation of PD Biomarkers in human whole blood

Whole blood was collected from six healthy donors and incubated with DMSO or 100 nmol/L AZD5153 for 2 hours at 37°C. The whole blood was transferred to PAXgene RNA tubes (BD Diagnostics), incubated for 2 hours at room temperature for RNA stabilization and stored at −20°C until RNA extraction. RNA extraction was performed using PAXgene Blood RNA kits (Qiagen) according to the manufacturer's instructions. Total RNA was then quantified, reverse transcribed, and used as template for quantitative PCR using primers (ABI) specific for MYC and HEXIM1. Data were normalized using GAPDH as the housekeeping gene and converted to relative signal $(2^{-\Delta Ct})^*100$ to calculate the percentage of control.

Results

AZD5153 is a potent BET bromodomain inhibitor possessing a bivalent binding mode

AZD5153, as shown in Fig. 1A, is a potent and selective BET bromodomain inhibitor. AZD5153 induces dimerization of Bromodomain 1 construct (BD1) of BRD4 in X-ray cocrystal structure (23). Additional biophysical characterization by analytical ultracentrifugation and small angle X-ray scattering demonstrated that AZD5153 can bind bivalently, namely, that one molecule of

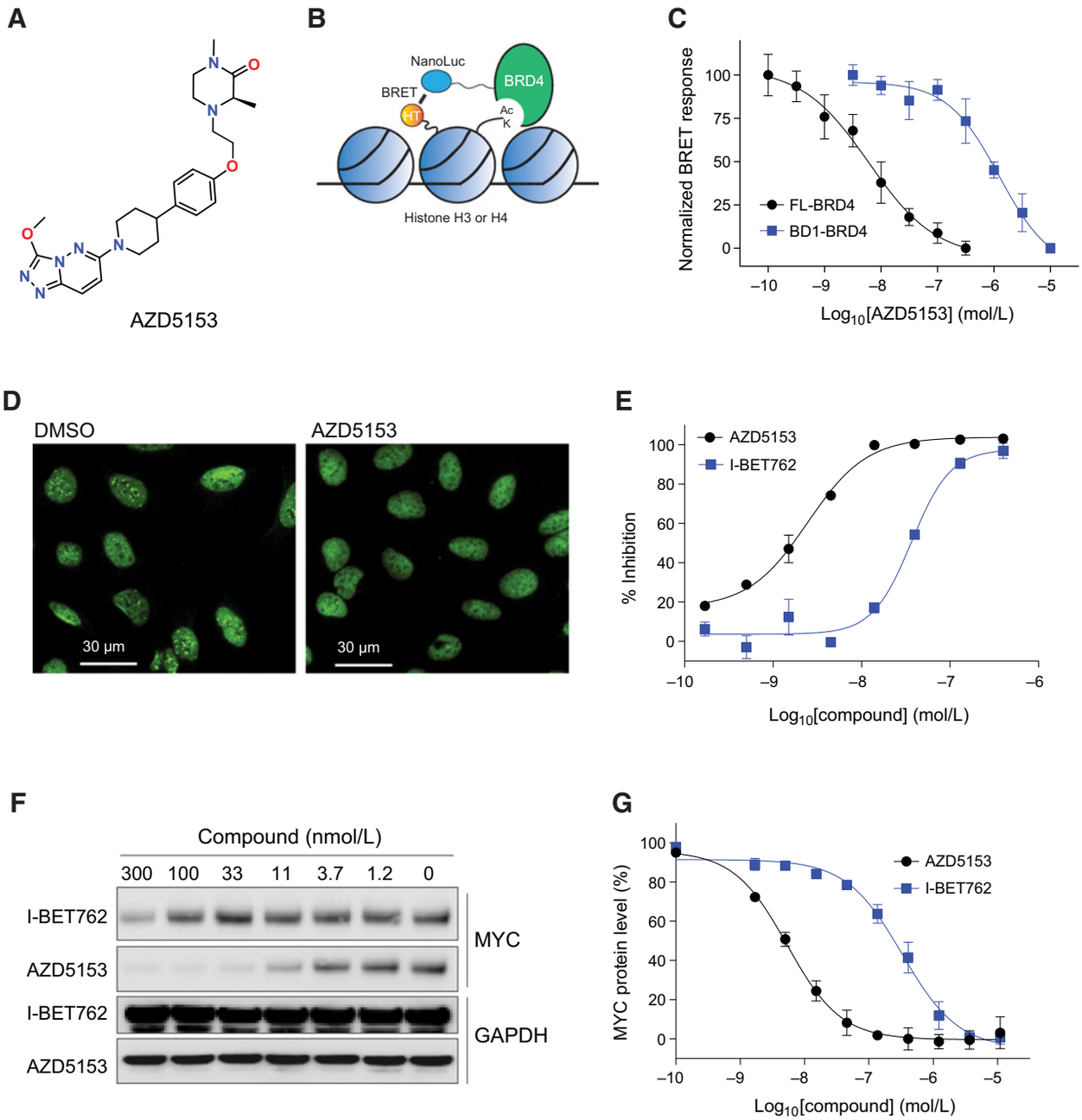

Figure 1.

AZD5153 is a potent BET bromodomain inhibitor possessing a bivalent binding mode. **A,** chemical structure of AZD5153. **B,** schematic of cellular nano-BRET assay system using full-length BRD4 (FL-BRD4) or BD1 domain-only BRD4 (BD1-BRD4) with a NanoLuc tag and histone H3.3 with a HaloTag in HCT116 cells. **C,** dose–response curves of AZD5153 displacing FL-BRD4 or BD1-BRD4 from histone H3.3 after 18 hours of treatment. **D,** formation of bright foci resulted from high level of BRD4 binding to the enhancer regions visualized by immunofluorescent staining in U2OS cells, and foci disruption by 4 hours treatment of 10 nmol/L AZD5153. **E,** dose–response curves of BRD4 foci inhibition with AZD5153 and monovalent inhibitor I-BET762. **F,** Western blots of MYC protein modulation by various concentrations of AZD5153 and I-BET762 in MM.1S cells with 4 hours of compound treatment. **G,** MYC modulation dose–response curves of AZD5153 and I-BET762 in MM.1S cells by quantitative flow cytometry analysis.

AZD5153 binds and ligates two bromodomains in BRD4 (data not shown), in contrast to other reported BET inhibitors such as JQ1 and I-BET762 that bind monovalently with one molecule binding to each bromodomain in BRD4.

To confirm the cell binding mode of AZD5153, we utilized a NanoBRET assay to monitor the interaction of BRD4 with chromatin using Halo-tagged histone H3 and a Nanoluciferase fusion protein with either the BD1 domain alone (BD1-BRD4)

or a full-length BRD4 construct (FL-BRD4; Fig. 1B; ref. 24). AZD5153 demonstrated a remarkable enhancement in potency for the displacement of full-length BRD4 relative to BD1, with IC_{50} values of 5.0 nmol/L and 1.6 μmol/L, for FL-BRD4 and BD1-BRD4, respectively (Fig. 1C). In contrast, the monovalent inhibitor, I-BET762, displaced both BD1 and full-length protein with comparable potency (200 nmol/L for BD1-BRD4 and 79 nmol/L for FL-BRD4; ref. 22). Further evidence of simultaneous engagement of BD1 and BD2 by AZD5153 was obtained by analogous experiments comparing wild-type FL-BRD4 to a bromodomain N433F mutant in which the BD2 function was abolished. AZD5153 demonstrated a drastically reduced IC_{50} value of 1.4 μmol/L in displacing mutant BRD4 from chromatin, in contrast to 8.7 nmol/L IC_{50} for wild-type protein (Supplementary Fig. S1A). In comparison, the monovalent inhibitor JQ1 showed a similar chromatin displacement dose-response between the mutant and wild-type protein (Supplementary Fig. S1B). Taken together, these data provide compelling evidence that the bivalent binding mode is the binding mechanism for AZD5153 in cells.

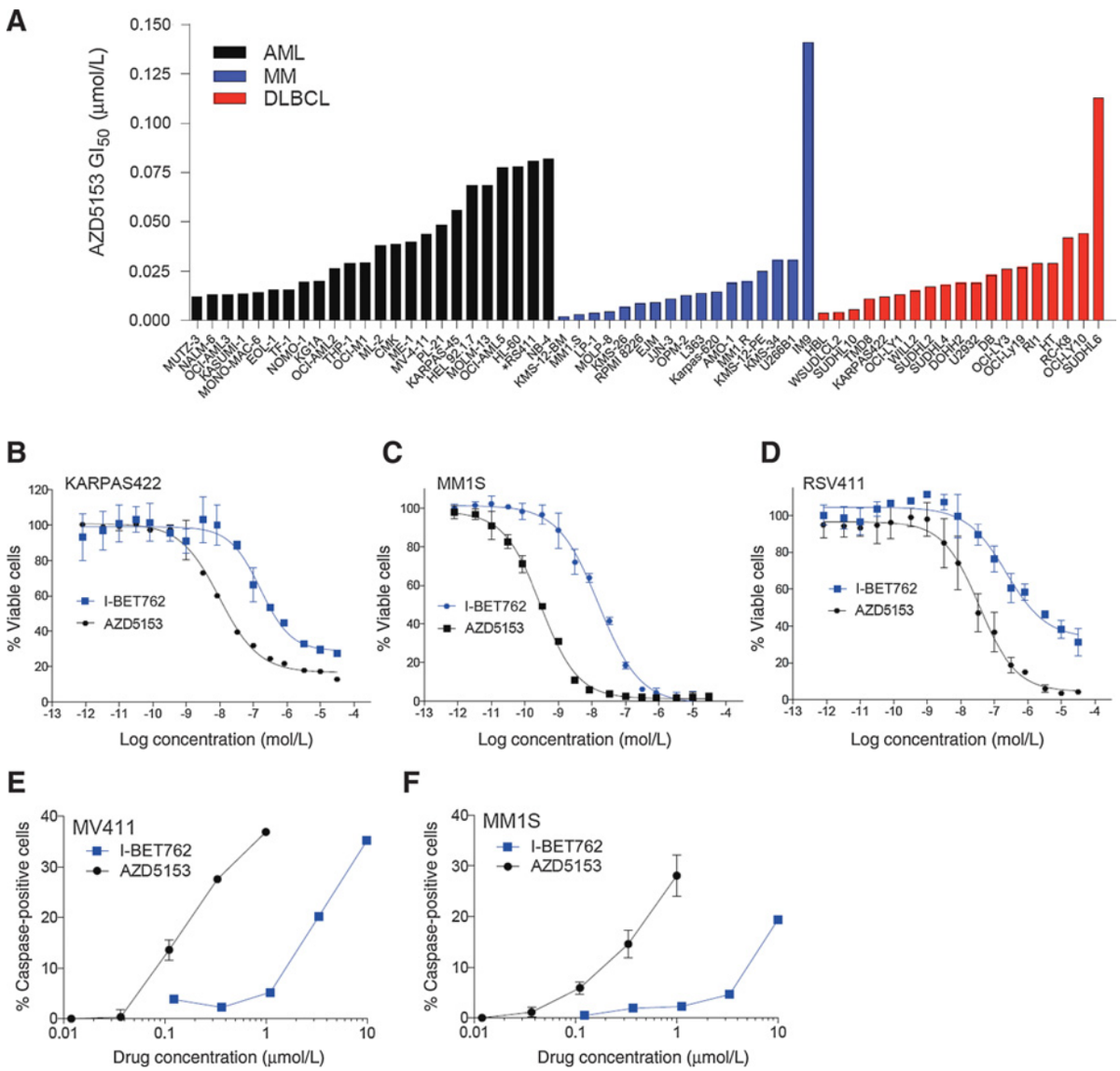

Figure 2.

AZD5153 exhibits broad antiproliferative activity against hematologic cancer cell lines. **A,** bar plot of GI_{50} values across a mixed panel of AML (black), MM (blue), and DLBCL (red) hematologic cancer cell lines following 72 hours treatment with AZD5153. Of note, *RS4;11 in the AML panel is actually an acute lymphoblastic leukemia (ALL) line. **B–D,** head-to-head comparison of cell viability dose–response curves of AZD5153 and I-BET762 in the indicated cell lines after 72 hours of treatment. **E** and **F,** apoptosis induction was assessed by measuring caspase-3–positive cell populations at various concentrations of AZD5153 and I-BET762 in the indicated cell lines 48 hours after compound treatment.

Avidity of bivalent binding leads to enhanced cellular potency with increased BRD4 displacement from chromatin and MYC modulation

We previously established a quantitative immunofluorescent assay to examine BRD4 chromatin displacement by measuring the disruption of BRD4 foci which are resulted from highly asymmetric binding of BRD4 to the enhancer regions (22). In this assay, AZD5153 potently disrupted BRD4 foci in U2OS cells with an IC_{50} value of 1.7 nmol/L (Fig. 1D–E). In contrast, the monovalent inhibitor I-BET762 had an IC_{50} of 36.0 nmol/L in the same assay (Fig. 1E).

To assess whether enhanced BRD4 bromodomain binding activity translated into modulation of downstream targets, we examined MYC protein modulation in a mixed panel of 14 hematologic tumor cell lines. AZD5153 efficiently downregulated MYC protein levels across the cell line panel irrespective of their sensitivity to AZD5153 (Supplementary Fig. S2). AZD5153 was more potent than the monovalent inhibitor I-BET762 in downregulating MYC protein, with 33 nmol/L of AZD5153 sufficient in reducing MYC to basal levels, whereas significant MYC remaining with 300 nmol/L of I-BET762 in MM1.S cells (Fig. 1F). This observation was further confirmed by quantitative flow cytometry, which determined a MYC protein modulation IC_{50} of 5.4 nmol/L for AZD5153, compared with an IC_{50} of 329 nmol/L for I-BET762 (Fig. 1G).

AML, MM, and DLBCL cell lines are highly sensitive to AZD5153

In order to assess the antiproliferative activity of AZD5153 in hematologic cancers, we tested a cell-line panel comprised of 60 AML, MM, and DLBCL cell lines. As shown in Fig. 2A, all cell lines tested exhibited exquisite sensitivity toward AZD5153 (GI_{50} < 150 nmol/L), with the majority of lines tested having a GI_{50} < 25 nmol/L. We hypothesized that the bivalent binding mode of AZD5153 could result in more robust target engagement and suppression of downstream effector pathways, collectively leading to an enhanced reduction in cell viability in select hematologic cancer subtypes. To test this hypothesis, five cell lines were treated with AZD5153 or I-BET762 for 72 hours and cell viability was measured. Across all five cell lines, the AZD5153 IC_{50} values were an average of 18-fold more potent than I-BET762 (Supplementary Fig. S3), with representative cell viability IC_{50} curves shown in Fig. 2B–D.

Although treatments with both drugs essentially eliminated all viable cells in MM cell lines as evidenced by the higher drug concentration points in the dose–response curves (Fig. 2C and Max% cell kill in Supplementary Fig. S3), AZD5153 reduced the level of remaining viable cells in KARPAS422, RS4;11, and JURKAT lines when the maximal drug effect of AZD5153 and I-BET762 demonstrated a plateau (Figs. 2B and D, and Max% cell kill in Supplementary Fig. S4). We deployed a flow cytometry assay to quantitatively measure caspase-3–positive cell populations in these cell lines to understand if a differential induction of apoptosis explained the difference observed in the cell viability assays. Unlike I-BET762, AZD5153 potently induces substantial apoptosis at 100 nmol/L in MV-4-11 and MM.1S cells (Fig. 2E and F). In summary, the avidity of bivalent target engagement by AZD5153 translated into deeper cellular responses in hematological cell lines.

AZD5153 modulates E2F, MYC, and mTOR transcriptional programs

To gain further understanding of the underlying cellular mechanism of phenotypic response and to facilitate biomarker discovery, we performed RNA sequencing on a panel of hematologic cancer cell lines (AML $n = 4$, MM $n = 5$, DLBCL $n = 2$) after treatment with AZD5153 (200 nmol/L) or DMSO vehicle for 24 hours (GSE85840). RNA sequencing analysis revealed 172 genes (109 downregulated and 63 upregulated genes) that were significantly modulated [$\log_2$ fold change > 1 and false discovery rate (FDR) < 0.05] across the cell line panel (Fig. 3A; Supplementary Table S2). Consistent with previous studies of BET inhibition, differential expression of HEXIM1, MYC, BCL2, FOSL1, and E2F1 was observed in select or multiple cell line types (16, 25–27). Gene Ontology (GO) analysis (28) was performed on the 109 uniformly downregulated transcripts by AZD5153. Genes involved in G_1–S transition and cell-cycle progression were highly enriched, suggesting that the intersecting genes function in core cellular processes (Supplementary Fig. S4). We used GSEA (29, 30) to gain a more comprehensive understanding of AZD5153 inhibitory effects on biological hallmarks and transcription factors using all cell line– and tumor-specific data ranked by differential expression. Significant gene sets identified in at least one comparison (FDR < 0.1) were ranked and represented by a heat map. Similar correlating hallmarks were noted across all tumor types and included transcriptional targets of MYC, E2F transcription factors, and mTOR signaling components (Fig. 3B–E).

Repression of mTOR signaling is an AZD5153 sensitivity correlate

In order to determine the consequences of BRD4 inhibition on protein levels, we used RPPA technology to quantitatively examine the expression of 182 total and phospho-proteins following 24 hours of AZD5153 treatment (200 nmol/L) in K562, IM9, MOLP8, MV-4-11, and OCILY19 cell lines (Supplementary Table S3). To identify protein modulation that correlated with sensitivity to AZD5153, we segregated cell lines into resistant (K562, IM9) and sensitive (MOLP8, MV-4-11, OCILY19) groups based on a GI_{50} cutoff of 100 nmol/L. Interestingly, RPPA revealed that cell lines sensitive to AZD5153 exhibited a marked decrease in the level of mTOR pathway–associated proteins following AZD5153 treatment (Fig. 4A). Selective downregulation of p-p70S6K, PRAS40, and p-4EBP1 in AZD5153-sensitive cell lines was confirmed by Western blot with multiple doses of AZD5153 (Fig. 4B). In contrast, MYC modulation was observed in both sensitive and resistant cell lines (Fig. 4B), suggesting that MYC downregulation was not sufficient to modulate cell survival. These data suggest that in hematologic malignancies, mTOR pathway downregulation may serve as an appropriate biomarker of sensitivity to BRD4 inhibitors such as AZD5153.

AZD5153 demonstrates potent antitumor activity in hematologic xenograft models

In order to assess the *in vivo* activity of AZD5153, we explored the effects of dosing AZD5153 in AML, MM, and DLBCL xenografts. MLL fusion leukemia has previously been shown to be dependent on BRD4 (26, 31). Thus, we chose a xenograft model of MV-4-11, an AML cell line that harbors an MLL-AF4 fusion oncogene, for initial *in vivo* efficacy experiments. A dose-dependent TGI was observed for 1, 2.5, and 5 mg/kg daily (QD) oral doses of AZD5153, ranging from 72% TGI for 1 mg/kg to regression for 5 mg/kg (Fig. 5A; Supplementary Fig. S5). A parallel experiment was carried out to further understand the dose–efficacy relationship for the lower end. Oral QD doses of 0.07, 0.36, and 0.72 mg/kg produced 16%, 23%, and 53% TGI,

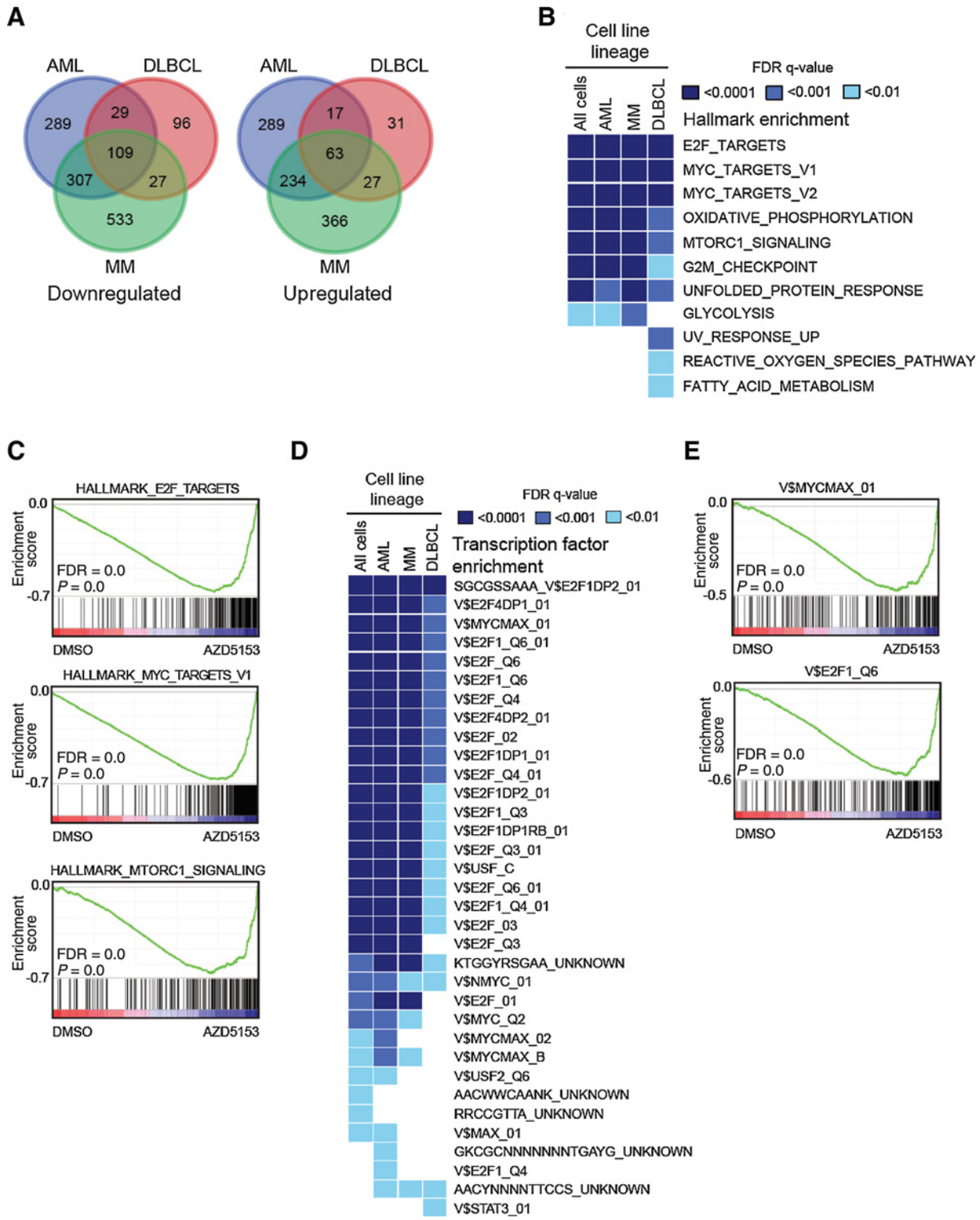

Figure 3.

RNA-seq analysis reveals downregulation of MYC, E2F, and mTOR target gene transcription by AZD5153. **A,** Venn diagram representation of the most downregulated and upregulated genes (FDR < 0.05 and $\log_2$ fold change > 1) following AZD5153 treatment for 24 hours in AML, MM, and DLBCL cell lines. **B,** heat maps of FDR (q < 0.01) values from GSEA of MSigDb transcription factor targets. Gene sets correlating with the AZD5153 phenotype are depicted. **C,** representative GSEA plots depicting gene sets most associated with AZD5153 downregulation from MSigDb. **D,** heat maps of FDR (q < 0.01) values from GSEA of hallmarks gene set collections. **E,** representative GSEA plots depicting gene sets most associated with AZD5153 downregulation from transcription factor target collections in all hematologic cell lines.

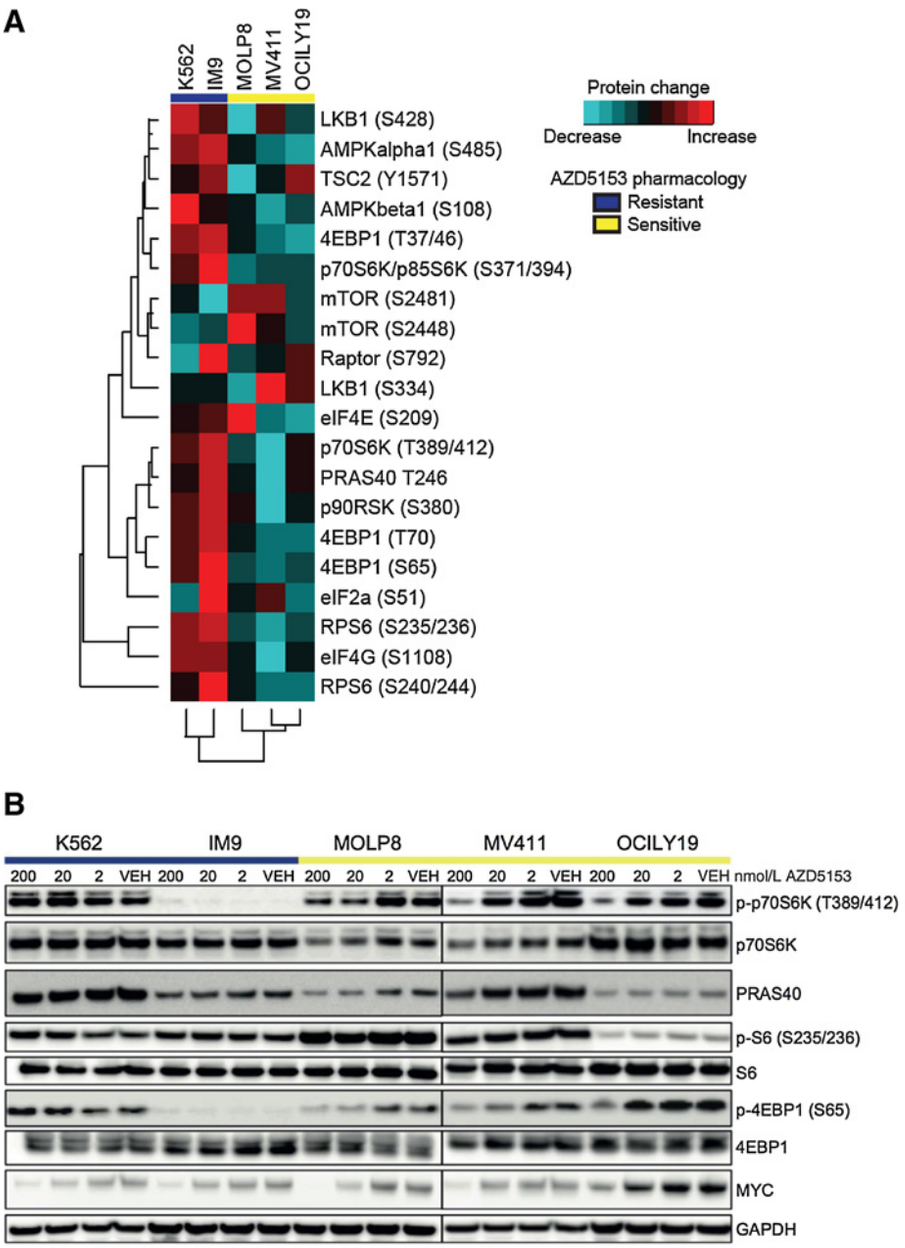

Figure 4.
Repression of mTOR signaling is an AZD5153 sensitivity correlate. **A,** unsupervised clustering heat map of mTOR-related total and phospho-proteins across five hematologic cell lines from RPPA analysis. Bar at the top of the heat map indicates whether a cell line was sensitive (yellow) or resistant (blue) to AZD5153. Individual protein values were generated by calculating the ratio of protein modulation at 24 hours between DMSO and AZD5153 (200 nmol/L) treatments. Turquoise, AZD5153-induced decreased expression; red, AZD5153-induced increased expression. Data are scaled according to z scores by protein. **B,** Western blot analysis of the change of protein level of select mTOR pathway signaling molecules and MYC by four concentrations of AZD5153 (0, 2, 20, and 200 nmol/L) after 24 hours of compound treatment across 5 hematological cell lines. Bar at the top of the Western blot indicates whether a cell line was sensitive (yellow) or resistant (blue) to AZD5153. Separation mark in the middle of Western blot indicates that this is a combined blot from two gels. Only one representative GAPDH loading control is shown.

respectively (Supplementary Fig. S5). To determine if AZD5153 had antitumor activity beyond MLL fusion AML, we tested it in additional xenograft models with known MYC or BRD4 linkage representing segments of MM, AML, and DLBCL. Treatment with 5 mg/kg QD, or a lower dose of 3.6 mg/kg for KARPAS422, resulted in 61% tumor regression in KMS11, 100% TGI in MOLP-8, 98% TGI in RS4;11, and 95% TGI in KARPAS-422 xenograft models (Figs. 5A–C; Supplementary Fig. S5). Interestingly, the AML model KG1a demonstrates similar *in vitro* potency to AZD5153 as the above models; however, it is less sensitive to AZD5153 *in vivo*. For example, a higher dose of 10 mg/kg QD resulted in moderate TGI of 74% (Fig. 2A; Supplementary Fig. S5). Understanding the difference between sensitivity *in vitro* and *in vivo* for KG1a would require further investigation. These data demonstrate AZD5153 is efficacious in a range of hematologic malignancies *in vivo*.

Duration of BRD4 inhibition is the driver for efficacy and sustained BRD4 inhibition led to near-complete tumor regression

In an effort to understand if increased daily target coverage could drive greater efficacy, we evaluated QD, BID, and continuous dosing delivered via a subcutaneous mini-pump in MV-4-11 tumor-bearing mice for 14 or 24 days. Increased efficacy was observed when AZD5153 was given BID at 1.25 or 2.5 mg/kg (split dose) compared with 2.5 or 5 mg/kg QD (Supplementary Fig. S5). The enhanced efficacy with BID dosing suggests that the duration of BRD4 target coverage is the driver for efficacy in the

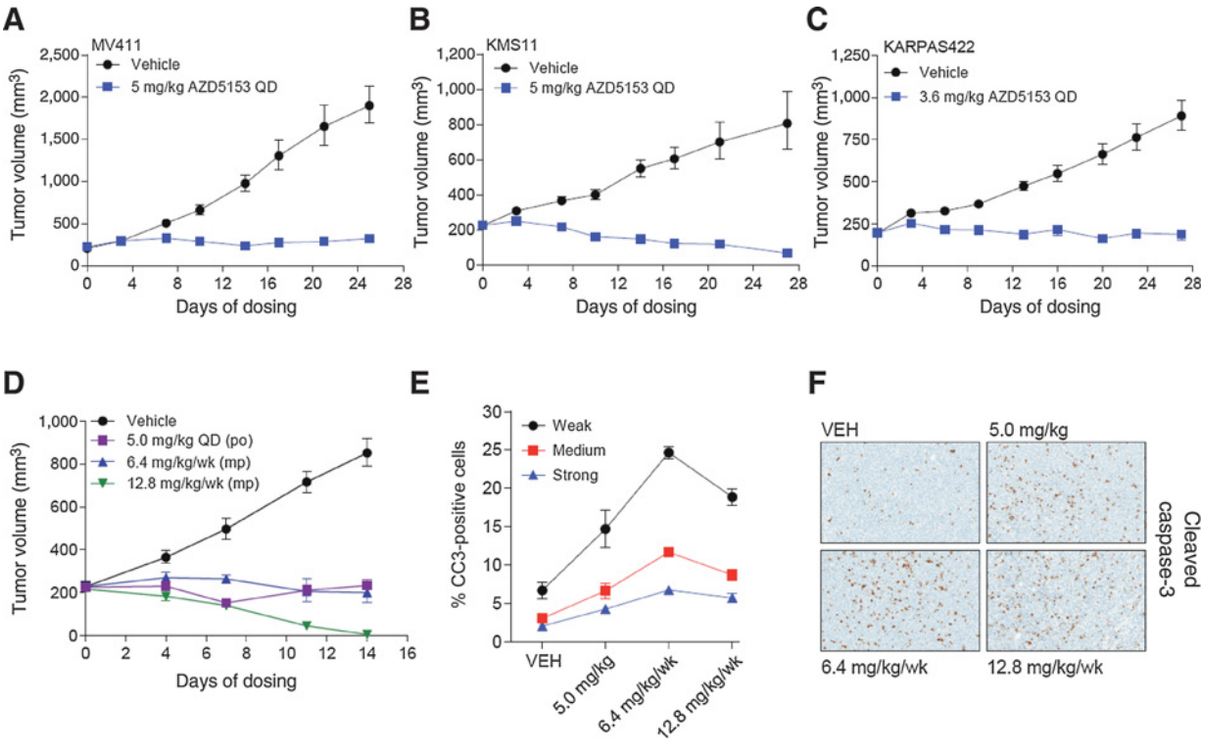

Figure 5.

AZD5153 is active in hematologic xenograft models. **A–C,** tumor growth curves with treatment of AZD5153 versus vehicle in representative tumor xenograft models of AML, MM, and DLBCL. Mice were treated daily with vehicle or oral dose of 3.6 or 5 mg/kg AZD5153. **D,** comparative antitumor effects with oral dose of 5 mg/kg/daily, continuous delivery of 6.4 mg/kg/wk or 12.8 mg/kg/wk via mini-pump, and vehicle. Black lines: vehicle-treated mice; blue, purple, and green lines: AZD5153-treated mice. **E,** quantified cleaved caspase-3 intensity from IHC in MV-4-11 tumors after 7 days of treatment. **F,** representative images of IHC used for image analysis showing increase in apoptoic cells after AZD5153 treatment.

MV-4-11 tumor model. Consistent with this notion, near complete regression (97%) of MV-4-11 tumors was achieved after 14 days of continuous delivery of AZD5153 at 12.8 mg/kg/week by mini-pump, with half of the dose at 6.4 mg/kg/week still resulting in tumor stasis (Fig. 5D). A higher oral dose of 5 mg/kg/daily, equivalent to 35 mg/kg/week, is needed to achieve a comparable efficacy to the 6.4 mg/kg/week continuous dose (Fig. 5D). The steady and prolonged BRD4 inhibition achieved with the mini-pump was associated with increased apoptosis in the tumors compared with daily oral dosing after 7 days of treatment (Fig. 5E and F). However, the 12.8 mg/kg/week mini-pump group, which was twice the efficacious dose of 6.4 mg/kg/week, was accompanied by significant body weight loss with an average weight loss of 10% observed. Taken together, these results support that the duration of BRD4 inhibition is the primary driver for *in vivo* efficacy, and additional dose/schedule investigation is needed to determine an appropriate balance of target coverage and tolerability to maximize the therapeutic benefit.

Pharmacodynamic evaluation in xenograft models and human whole blood supports MYC and HEXIM1 as biomarkers for AZD5153 inhibition

To understand the pharmacokinetic (PK)/PD relationship of AZD5153, MYC mRNA and protein levels were measured by quantitative PCR (qPCR) and Western blot. The concentration of AZD5153 was also measured in the plasma of the corresponding mouse after a single oral dose of 2.5, 5, or 10 mg/kg in MV-4-11 xenografts. All three doses induced significant modulation of MYC mRNA and protein over the first 8 hours but largely recovered by 16 hours (Fig. 6A and D). There was an inverse correlation between AZD5153 concentration in plasma and MYC mRNA levels in tumors (Fig. 6A). Significant inhibition of MYC mRNA was achieved with free plasma concentration as low as 0.1 μmol/L of AZD5153 in mice with MV-4-11 tumors. The MYC mRNA levels returned to baseline as AZD5153 was cleared from the plasma. In contrast, HEXIM1 mRNA was upregulated by AZD5153 treatment and had a similar but inverse PK/PD relationship (data not shown). An example of such a relationship is shown in Fig. 6F, when mRNA levels of MYC and HEXIM1 were determined at 2 hours after the 5 mg/kg dose, MYC mRNA was downregulated by about 80% whereas HEXIM1 mRNA was upregulated by 400% (Fig. 6F).

To confirm MYC protein modulation by AZD5153 and understand the heterogeneity within the tumors, immunohistochemistry (IHC) was performed in MV-4-11 tumors after 20 mg/kg dosing. As shown in Fig. 6B and C, the vehicle-treated tumor samples have 40% of cells with strong or medium MYC staining with the remaining 60% of cells having weak or no MYC staining. Acute oral administration of 20 mg/kg AZD5153 greatly reduced the number of cells with strong or medium intensity of MYC (97% and 75% reduction, respectively) at 2 hours post dosing. Correlating with PK, MYC staining intensity began to recover at 8 hours,

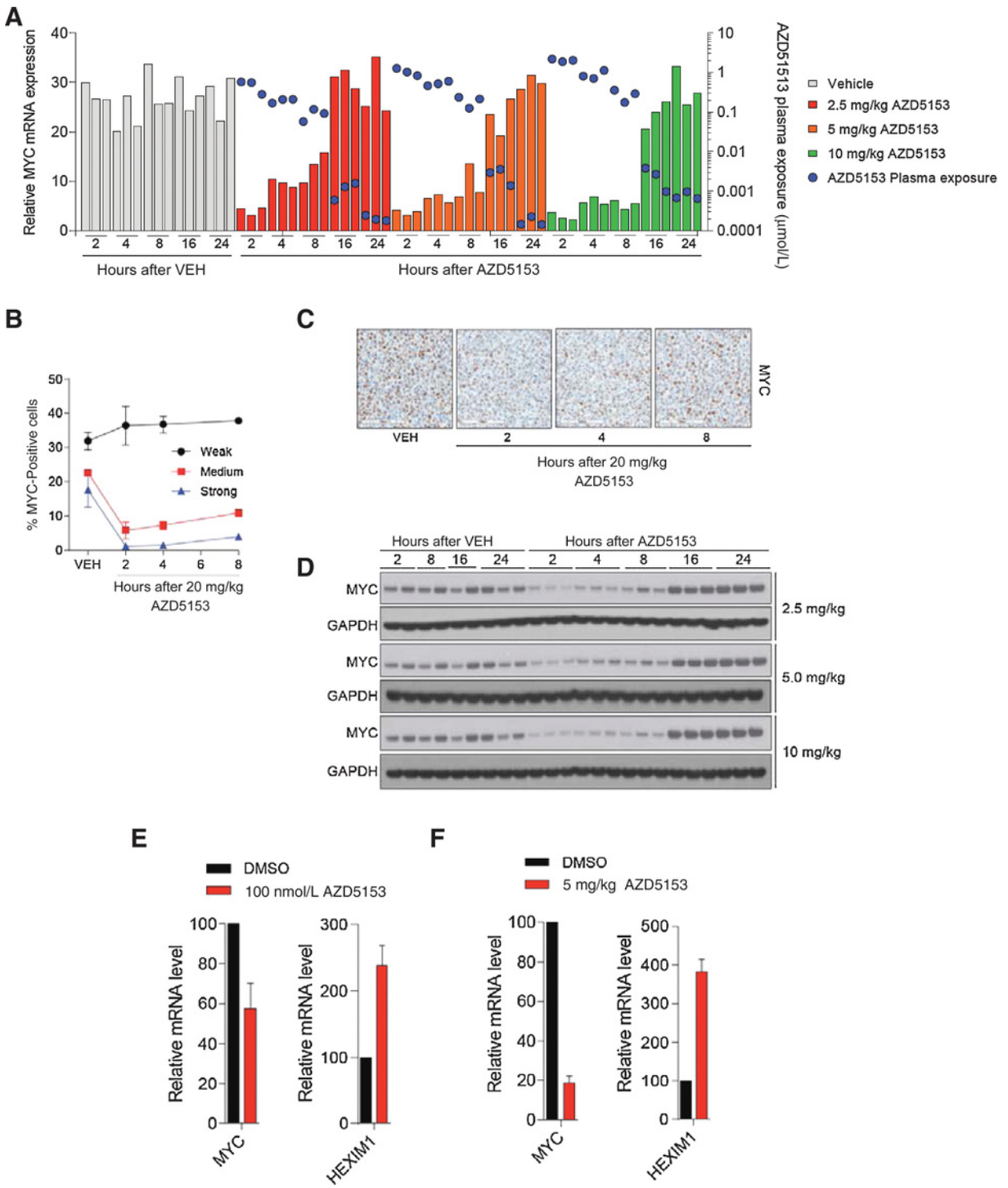

Figure 6.

AZD5153 modulates MYC and HEXIM1 in AML xenograft tumors and human whole blood. **A,** relationship of MYC mRNA levels in MV-4-11 tumors and AZD5153 concentration in mouse plasma at three dose levels of AZD5153. Each bar represents an individual mouse. **B,** IHC quantifying the percentage of MV-4-11 tumor cells with different levels of MYC staining intensity (weak, medium and strong) over time after a single oral 20 mg/kg dose of AZD5153. **C,** representative MYC IHC images used for analysis. The heterogeneity of MYC staining intensity is apparent in each tumor section. **D,** Western blot for MYC expression in same tumors used for mRNA analysis shown in **A**. **E,** modulation of MYC and HEXIM1 mRNA in human whole blood after *ex vivo* treatment with 100 nmol/L AZD5153. Blood samples were obtained from normal healthy volunteers. Error bars, ± SEM. **F,** modulation of MYC and HEXIM1 mRNA in MV-4-11 xenograft tumor tissue 2 hours after the 5 mg/kg oral dose.

the last time point taken in the study (Fig. 6B and C). Interestingly, there were a significant number of cells with medium MYC staining remaining throughout the time points, highlighting the heterogeneity nature of response, a phenomenon that is frequently observed in the treatment of patient tumors.

Due to the limited availability of paired tumor biopsy samples during clinical development of novel agents, PD assessment with tumor tissue is not always achievable. Therefore, we evaluated AZD5153 induced mRNA expression changes in whole blood as a surrogate PD endpoint. To identify potential clinical PD biomarkers, the mRNA expression of MYC and HEXIM1 genes were evaluated in human whole blood from healthy volunteers. Treatment with 100 nmol/L AZD5153 for 2 hours resulted in 42% decrease of MYC and 240% increase of HEXIM1 mRNA (Fig. 6E), similar to observation in MV-4-11 tumor tissue (Fig. 6F). These data support the evaluation of these two biomarkers, together with other novel candidates that are described elsewhere (32), as potential human whole blood PD biomarkers in clinical trials.

Discussion

Herein, we assessed the characteristics of AZD5153, a novel BET bromodomain inhibitor. The bivalent binding mode of AZD5153 sets it apart from previously described BET bromodomain inhibitors. Mechanistically, the simultaneous ligation of both BRD4 bromodomains by AZD5153 allows for efficient displacement of BRD4 from chromatin at lower drug concentrations. This unique biophysical property translates into enhanced *in vitro* and *in vivo* pharmacologic activity.

In the hematologic tumor setting, our comparative efficacy studies with QD, BID, and continuous dosing of AZD5153 have revealed that duration of target coverage is the primary driver for *in vivo* efficacy. Twice-daily dosing with the split QD dose mitigated the issue of fast clearance of AZD5153 from the mouse system and provided longer duration of target inhibition translating into better efficacy. We enhanced these findings by using mini-pump drug infusion, which eliminates PK fluctuations and provides consistent target inhibition. Compared with daily oral dosing, less than one fifth of AZD5153 was needed per week via mini-pump to achieve comparable efficacy. Furthermore, our data indicate C_{max} does not play a significant role in driving AZD5153 efficacy. Namely, there was a greater than 12-fold difference in C_{max} between 5 mg/kg/daily oral and 6.4 mg/kg/week mini-pump infusion. Unfortunately, enhanced efficacy achieved through prolonged target inhibition was often accompanied by significant body weight loss, which we used as a surrogate for gastrointestinal toxicity for BET inhibitors in mice. However, there remains a therapeutic index at lower doses using continuous infusion or a daily oral schedule, thus allowing for antitumor activity without concomitant bodyweight loss. Sustained BRD4 inhibition for a period of 2 to 3 days could lead to *in vitro* cell death of MV-4-11 cancer cells via apoptosis, suggesting that an intermittent schedule is sufficient to deliver efficacy. Further investigation is needed to validate if such a schedule can sufficiently induce tumor cell death, while minimizing toxicity within normal tissues. Moreover, BET bromodomain inhibitors may have different scheduling requirements in solid tumor settings, owing to differences in tumor biology and microenvironment. A systematic investigation of both dose and schedule will be required to find the appropriate balance of drug exposure, efficacy, and tolerability for the myriad of disease subtypes for which BRD4 is being prosecuted as a cancer drug target. Ongoing clinical studies will no doubt be critical to define the optimal use of the BET bromodomain inhibitors.

Our gene expression analysis characterized the transcriptional response induced by AZD5153 in AML, MM, and DLBCL. Consistent with previously described studies examining BET bromodomain inhibitors, we observed significant modulation of MYC and E2F gene programs. However, our study is the first, to our knowledge, to reveal a significant modulation of an mTOR gene signature in these tumor types. Furthermore, we demonstrated that modulation of the mTOR signaling correlates with sensitivity to AZD5153 in cell lines we studied, whereas MYC levels do not. Our data suggest that modulation of the mTOR pathway, which is widely deregulated in many hematological cancers, contributes to the broad anticancer phenotype that we and others have observed for BET inhibitors in preclinical hematological cancer models. Consistent with this observation, the clinical candidate BET inhibitor, OTX015, exhibits synergy when combined with everolimus in DLBCL (33). We speculate that downregulation of mTOR signaling components may serve as a correlative biomarker for future clinical studies of AZD5153 and/or other clinical candidate BET bromodomain inhibitors.

Both MYC mRNA and protein exhibited a concentration-dependent decrease in response to AZD5153 in both cell and *in vivo* models of hematological malignancies. Furthermore, inhibition of MYC mRNA was also observed in treated human whole blood and corresponded with an induction of HEXIM1 expression, supporting the use of these readouts as potential clinical biomarkers of target engagement for AZD5153. In the clinical setting, the use of human whole blood as a means to demonstrate target engagement could be beneficial, especially when paired tumor biopsies are not available.

In summary, AZD5153 is a novel BET bromodomain inhibitor with a bivalent binding mode. The unique biophysical properties of AZD5153 offer potency and pharmacological advantages over traditional monovalent BET bromodomain inhibitors. Based on potent *in vivo* antitumor activity, AZD5153 is a promising drug candidate for the treatment of hematological malignancies.

Disclosure of Potential Conflicts of Interest

Y. Yao reports receiving other commercial research support from and has ownership in stock from AstraZeneca. A. Dulak reports receiving other commercial research support from Astrazeneca. S. Boiko reports receiving a commercial research grant from AstraZeneca. T. Cheung reports receiving other commercial research support from and has ownership interest (including patents) in AstraZeneca. G.B. Mills reports receiving commercial research grant from, has received speakers bureau honoraria from, and is a consultant/advisory board member for AstraZeneca. M.J. Waring is a professor at Newcastle University and reports receiving other commercial research support from AstraZeneca. M. Zinda reports receiving other commercial research support from and has ownership interest (including patents) in AstraZeneca. E. Clark has ownership interest (including patents) in the AstraZeneca. H. Chen reports receiving other commercial research support from and has ownership interest (including patents) in the AstraZeneca. No potential conflicts of interest were disclosed by the other authors.

Authors' Contributions

Conception and design: G.W. Rhyasen, M.M. Hattersley, A. Dulak, G. Walker, T.C. Yeh, A.A. Rabow, J.R. Dry, P. Lyne, G.B. Mills, S.E. Fawell, M.J. Waring, M. Zinda, H. Chen

Development of methodology: M.M. Hattersley, Y. Yao, P. Petteruti, I.L. Dale, S. Boiko, S. Wen, D. Lawson, M. Collins, L. Bao, G. Walker, G. O'Connor, J.R. Dry

Acquisition of data (provided animals, acquired and managed patients, provided facilities, etc.): M.M. Hattersley, Y. Yao, W. Wang, P. Petteruti,

S. Boiko, S. Wen, L. Castriotta, M. Collins, L. Bao, G. Walker, G. O'Connor, A.A. Rabow, G.B. Mills, M. Zinda

Analysis and interpretation of data (e.g., statistical analysis, biostatistics, computational analysis): G.W. Rhyasen, M.M. Hattersley, Y. Yao, A. Dulak, W. Wang, P. Petteruti, I.L. Dale, S. Boiko, J. Zhang, L. Castriotta, M. Collins, M.J. Ahdesmaki, G. Walker, G. O'Connor, T.C. Yeh, A.A. Rabow, C. Reimer, G.B. Mills, S.E. Fawell, M.J. Waring, E. Clark, H. Chen

Writing, review, and/or revision of the manuscript: G.W. Rhyasen, M.M. Hattersley, Y. Yao, A. Dulak, W. Wang, I.L. Dale, S. Boiko, T. Cheung, J. Zhang, G. Walker, T.C. Yeh, A.A. Rabow, C. Reimer, G.B. Mills, S.E. Fawell, M.J. Waring, M. Zinda, E. Clark, H. Chen

Administrative, technical, or material support (i.e., reporting or organizing data, constructing databases): G.W. Rhyasen, Y. Yao, D. Lawson, M.J. Waring

Study supervision: M.M. Hattersley, G. Walker, T.C. Yeh, J.R. Dry, C. Reimer, E. Clark, H. Chen

Acknowledgments

We thank Promega Corporation for performing mutant BRD4 cellular assays; Justin Cidado and Deepa Bhavsar for generating cell panel data; Galina Repik for assistance in cell line banking and retrieval.

The costs of publication of this article were defrayed in part by the payment of page charges. This article must therefore be hereby marked *advertisement* in accordance with 18 U.S.C. Section 1734 solely to indicate this fact.

Received March 14, 2016; revised June 29, 2016; accepted August 15, 2016; published OnlineFirst August 29, 2016.

References

1. Dhalluin C, Carlson JE, Zeng L, He C, Aggarwal AK, Zhou MM. Structure and ligand of a histone acetyltransferase bromodomain. Nature 1999;399:491–6.
2. Moriniere J, Rousseaux S, Steuerwald U, Soler-Lopez M, Curtet S, Vitte AL, et al. Cooperative binding of two acetylation marks on a histone tail by a single bromodomain. Nature 2009;461:664–8.
3. Dey A, Chitsaz F, Abbasi A, Misteli T, Ozato K. The double bromodomain protein Brd4 binds to acetylated chromatin during interphase and mitosis. Proc Natl Acad Sci U S A 2003;100:8758–63.
4. Filippakopoulos P, Picaud S, Mangos M, Keates T, Lambert JP, Barsyte-Lovejoy D, et al. Histone recognition and large-scale structural analysis of the human bromodomain family. Cell 2012;149:214–31.
5. Dey A, Nishiyama A, Karpova T, McNally J, Ozato K. Brd4 marks select genes on mitotic chromatin and directs postmitotic transcription. Mol Biol Cell 2009;20:4899–909.
6. Jang MK, Mochizuki K, Zhou M, Jeong HS, Brady JN, Ozato K. The bromodomain protein Brd4 is a positive regulatory component of P-TEFb and stimulates RNA polymerase II-dependent transcription. Mol Cell 2005;19:523–34.
7. Yang Z, Yik JH, Chen R, He N, Jang MK, Ozato K, et al. Recruitment of P-TEFb for stimulation of transcriptional elongation by the bromodomain protein Brd4. Mol Cell 2005;19:535–45.
8. Hnisz D, Abraham BJ, Lee TI, Lau A, Saint-Andre V, Sigova AA, et al. Super-enhancers in the control of cell identity and disease. Cell 2013;155:934–47.
9. Loven J, Hoke HA, Lin CY, Lau A, Orlando DA, Vakoc CR, et al. Selective inhibition of tumor oncogenes by disruption of super-enhancers. Cell 2013;153:320–34.
10. Nicodeme E, Jeffrey KL, Schaefer U, Beinke S, Dewell S, Chung CW, et al. Suppression of inflammation by a synthetic histone mimic. Nature 2010;468:1119–23.
11. Filippakopoulos P, Qi J, Picaud S, Shen Y, Smith WB, Fedorov O, et al. Selective inhibition of BET bromodomains. Nature 2010;468:1067–73.
12. Shi J, Vakoc CR. The mechanisms behind the therapeutic activity of BET bromodomain inhibition. Mol Cell 2014;54:728–36.
13. Roe JS, Mercan F, Rivera K, Pappin DJ, Vakoc CR. BET bromodomain inhibition suppresses the function of hematopoietic transcription factors in acute myeloid leukemia. Mol Cell 2015;58:1028–39.
14. Chng WJ, Huang GF, Chung TH, Ng SB, Gonzalez-Paz N, Troska-Price T, et al. Clinical and biological implications of MYC activation: a common difference between MGUS and newly diagnosed multiple myeloma. Leukemia 2011;25:1026–35.
15. Brioli A, Melchor L, Walker BA, Davies FE, Morgan GJ. Biology and treatment of myeloma. Clin Lymphoma Myeloma Leukemia 2014;14: S65–70.
16. Delmore JE, Issa GC, Lemieux ME, Rahl PB, Shi J, Jacobs HM, et al. BET bromodomain inhibition as a therapeutic strategy to target c-Myc. Cell 2011;146:904–17.
17. Lenz G, Staudt LM. Aggressive lymphomas. N Engl J Med 2010; 362:1417–29.
18. Basso K, Dalla-Favera R. Roles of BCL6 in normal and transformed germinal center B cells. Immunol Rev 2012;247:172–83.
19. Slack GW, Gascoyne RD. MYC and aggressive B-cell lymphomas. Adv Anat Pathol 2011;18:219–28.
20. Monti S, Chapuy B, Takeyama K, Rodig SJ, Hao Y, Yeda KT, et al. Integrative analysis reveals an outcome-associated and targetable pattern of p53 and cell cycle deregulation in diffuse large B cell lymphoma. Cancer Cell 2012;22:359–72.
21. Chapuy B, McKeown MR, Lin CY, Monti S, Roemer MG, Qi J, et al. Discovery and characterization of super-enhancer-associated dependencies in diffuse large B cell lymphoma. Cancer Cell 2013;24: 777–90.
22. Waring MJ, Chen H, Rabow AA, Walker GE, Bobby R, Boiko S, et al. Bivalent binding to BET bromodomains. Nat Chem Biol 2016, In press.
23. Bradbury RH, Callis R, Carr GR, Chen H, Clark E, Feron L, et al. Optimization of a series of bivalent triazolopyridazine based BET bromodomain inhibitors: the discovery of (3R)-4-[2-[4-[1-(3-methoxy-[1,2,4]triazolo[4,3-b]pyridazin-6-yl)-4-piperidyl]phenoxy]ethyl]-1,3-dimethyl-piperazin-2-one(AZD5153). J Med Chem 2016;59:7801–17.
24. Machleidt T, Woodroofe CC, Schwinn MK, Méndez J, Robers MB, Zimmerman K, et al. NanoBRET—A novel BRET platform for the analysis of protein-protein interactions. ACS Chem Biol 2015;10:1797–804.
25. Bartholomeeusen K, Xiang Y, Fujinaga K, Peterlin BM. Bromodomain and extra-terminal (BET) bromodomain inhibition activate transcription via transient release of positive transcription elongation factor b (P-TEFb) from 7SK small nuclear ribonucleoprotein. J Biol Chem 2012; 287:36609–16.
26. Dawson MA, Prinjha RK, Dittmann A, Giotopoulos G, Bantscheff M, Chan WI, et al. Inhibition of BET recruitment to chromatin as an effective treatment for MLL-fusion leukaemia. Nature 2011;478:529–33.
27. Baker EK, Taylor S, Gupte A, Sharp PP, Walia M, Walsh NC, et al. BET inhibitors induce apoptosis through a MYC independent mechanism and synergise with CDK inhibitors to kill osteosarcoma cells. Sci Rep 2015;5:10120.
28. Chen EY, Tan CM, Kou Y, Duan Q, Wang Z, Meirelles GV, et al. Enrichr: interactive and collaborative HTML5 gene list enrichment analysis tool. BMC Bioinformatics 2013;14:128.
29. Subramanian A, Tamayo P, Mootha VK, Mukherjee S, Ebert BL, Gillette MA, et al. Gene set enrichment analysis: a knowledge-based approach for interpreting genome-wide expression profiles. Proc Natl Acad Sci U S A 2005;102:15545–50.
30. Mootha VK, Lindgren CM, Eriksson KF, Subramanian A, Sihag S, Lehar J, et al. PGC-1alpha-responsive genes involved in oxidative phosphorylation are coordinately downregulated in human diabetes. Nat Genet 2003;34: 267–73.
31. Zuber J, Shi J, Wang E, Rappaport AR, Herrmann H, Sison EA, et al. RNAi screen identifies Brd4 as a therapeutic target in acute myeloid leukaemia. Nature 2011;478:524–8.
32. Yeh TC, O'Connor G, Petteruti P, Dulak A, Hattersley MM, Barrett C, et al. Identification of CCR2 and CD180 as robust pharmacodynamic tumor and blood biomarkers for clinical use with BRD4/BET inhibitors. Clinical Cancer Research. In press 2016.
33. Boi M, Gaudio E, Bonetti P, Kwee I, Bernasconi E, Tarantelli C, et al. The BET Bromodomain Inhibitor OTX015 affects pathogenetic pathways in preclinical B-cell tumor models and synergizes with targeted drugs. Clin Cancer Res 2015;21:1628–38.